Supplementary information for: Choice-related activity and correlated noise in subcortical vestibular neurons

SHENG LIU[1,3], YONG GU[1], GREGORY C. DEANGELIS[2] AND DORA E. ANGELAKI[1,3]

[1]Dept. of Neurobiology, Washington University School of Medicine, St. Louis, MO

[2]Dept. of Brain and Cognitive Sciences, University of Rochester, Rochester NY

[3]Department of Neuroscience, Baylor College of Medicine, Houston TX

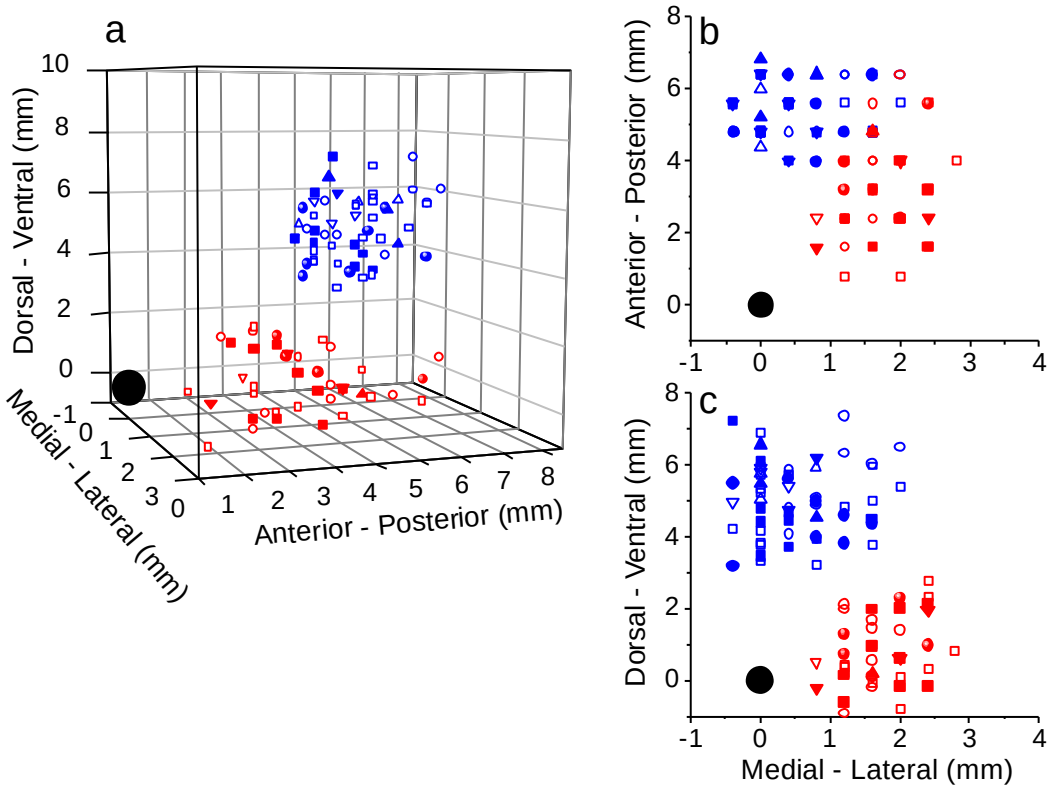

Suppl. Fig. 1. Three-dimensional reconstruction of recording sites. Recording sites of cerebellar nuclei (CBN, blue) and vestibular nuclei (VTN, red) neurons from 4 animals (denoted by different symbols). **(a)** Three dimensional illustration of recording sites. **(b)** Recording locations projected onto the horizontal plane. **(c)** Recording locations projected onto the coronal plane. Filled symbols: cells with significant ($p<0.05$) choice probabilities; open symbols: cells with choice probabilities that are not significant ($p>0.05$). The large black circle marks the location of the abducens nucleus, and was taken as the origin of the coordinate frame shown here.

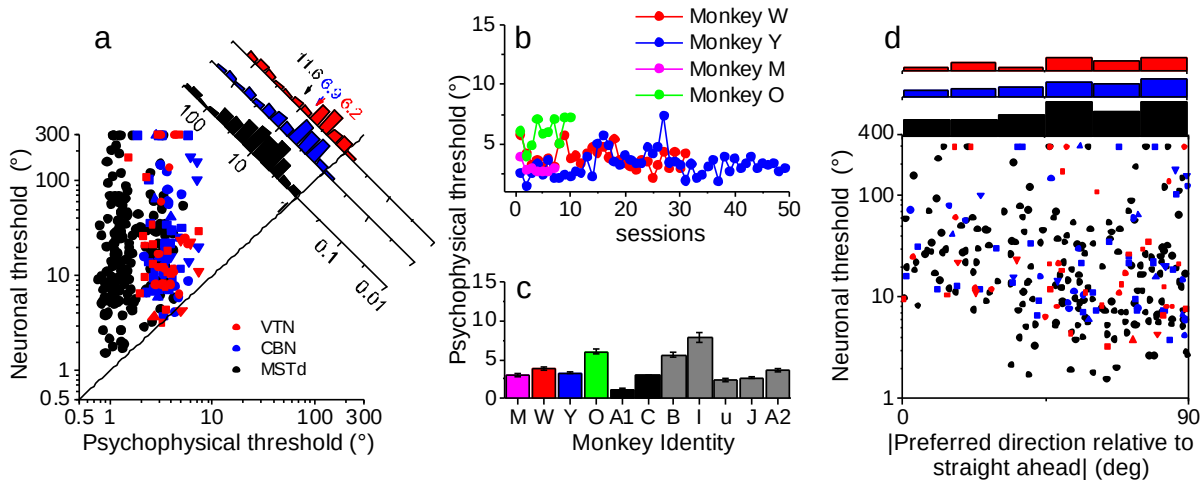

Suppl. Fig. 2. Summary of neuronal and behavioral sensitivity. (a) Comparison of psychophysical and neuronal thresholds for each experimental session (CBN: blue, VTN: red, and MSTd: black). The diagonal histogram shows the distribution of neuronal to psychophysical (N/P) threshold ratios. Arrows illustrate mean N/P ratios. **(b)** Psychophysical thresholds as a function of recording session, separately for each of the 4 animals used for the VTN/CBN recordings. Note that all recording sessions were conducted after training was complete. There is no significant trend for psychophysical thresholds to change across recording sessions, confirming that the animals had reached asymptotic performance when recordings commenced (monkey W: r=-0.26, p = 0.15, n =31; monkey Y: r=0.16, p = 0.25, n =49; monkey M: r=-0.32, p = 0.5, n =7; monkey O: r=0.6, p = 0.07, n =10). **(c)** Comparison of mean psychophysical thresholds (±SE) for the 4 VTN/CBN animals (colored bars), the two MSTd animals (black bars), and 5 other animals (from previous studies) that also performed the vestibular heading discrimination task. Note that the thresholds of the 4 VTN/CBN animals were well within the range of thresholds seen in other animals, however one of the MSTd animals (A1) had unusually low heading thresholds compared to the rest of the animals (see also panel a). The range of thresholds in our monkeys is also similar to human thresholds in a similar task performed using an identical motion platform. **(d)** Dependence of neuronal thresholds on preferred direction relative to straight ahead. For each cell, neural threshold is plotted against the absolute difference between the cell's preferred direction and the straight-ahead direction (heading=0°). The plot was folded around the 90° difference value to facilitate regression analysis. There is a significant correlation between neuronal threshold and heading preference for MSTd, but not for VTN and CBN (Spearman correlation, MSTd: R = -0.27, p < 0.01; VTN: R = -0.19, p = 0.2; CBN: R = -0.14, p = 0.3). This correlation approaches significance when data from VTN and CBN are pooled (R=-0.17, p = 0.08). Marginal distributions of the relative direction difference are also shown (top), separately for CBN (blue), VTN (red) and MSTd (black). There was no significant difference between the VTN/CBN and MSTd distributions of direction preferences (p>0.6, Kolmogorov-Smirnov tests). For VTN/CBN, different symbols mark data from different animals (upward triangles: monkey M, n=7; circles: monkey W, n=31; squares: monkey Y, n=49 ; downward triangles: monkey O, n=10).

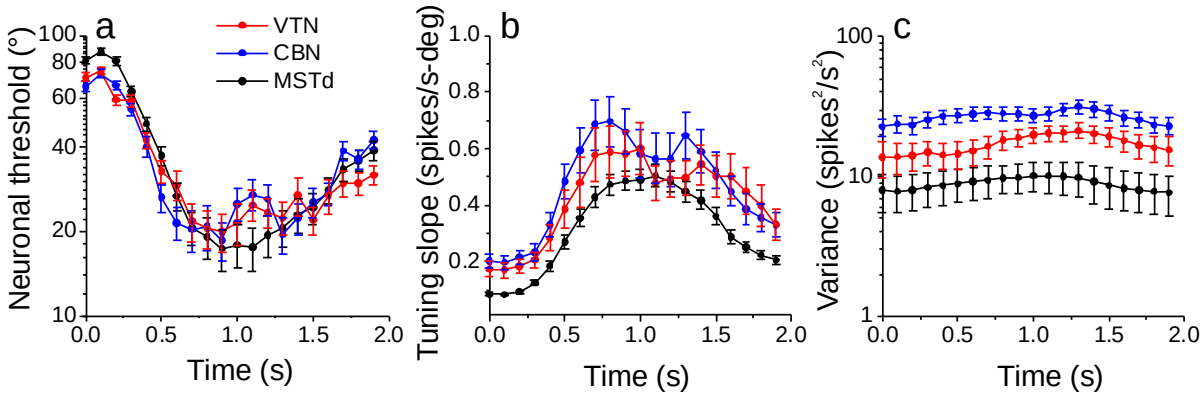

Suppl. Fig. 3. Time course of variations in neuronal thresholds (a), tuning curve slopes (b) and response variance (c). CBN: blue (n=56); VTN: red (n=41); MSTd: black (n=183). Tuning curve slope was calculated from linear regression between neuronal responses and heading direction during the discrimination task. Response variance was computed only from the 0° heading data. Each point in these plots represents data obtained from a 400ms analysis window that was shifted across time by multiples of 100ms. Error bars illustrate s.e.m.

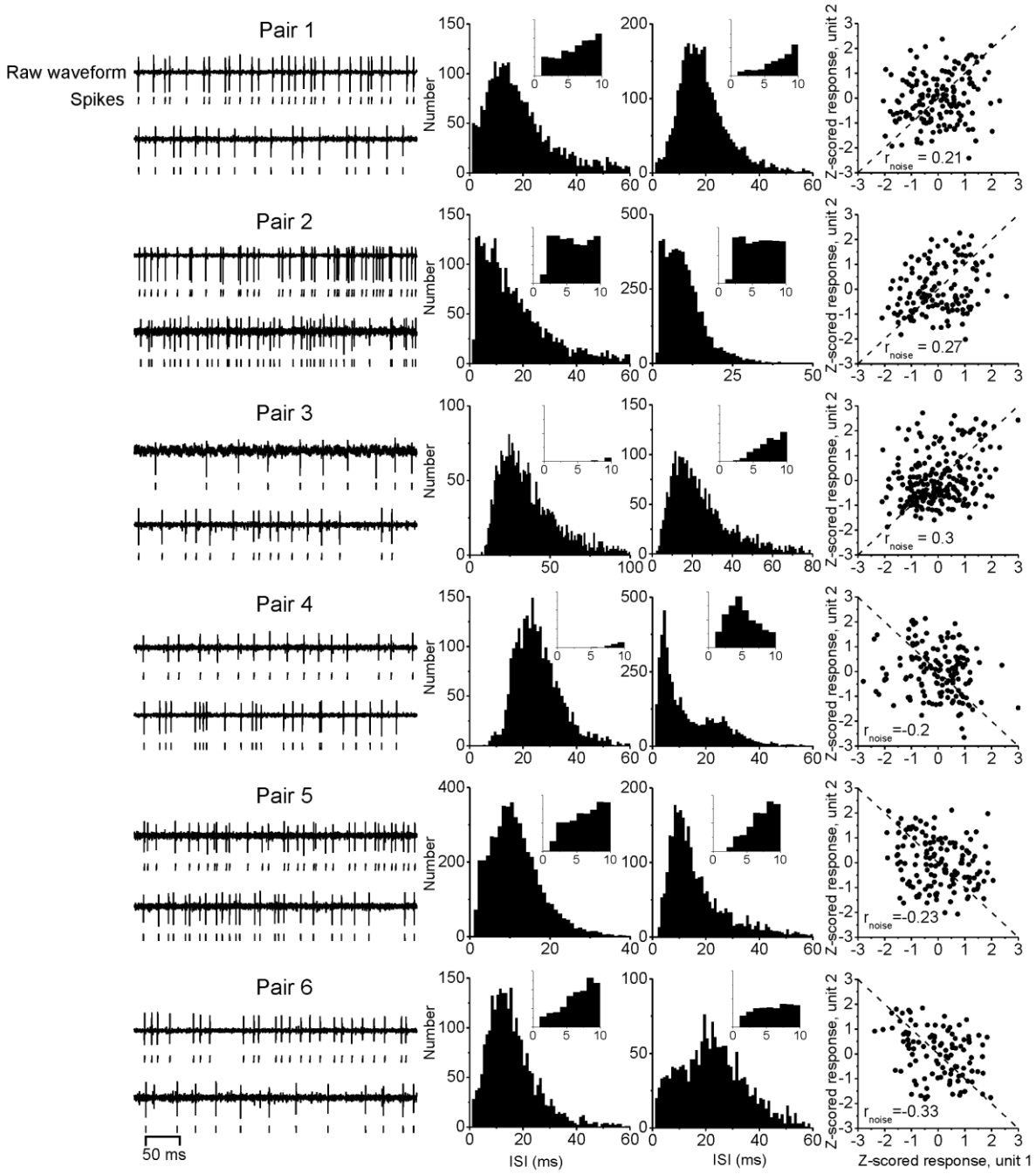

Suppl. Fig. 4. Raw data from 6 pairs of simultaneously-recorded VTN or CBN neurons with significant noise correlations. (a) For each of the 6 pairs of neurons, a segment of the digitized raw neural voltage signals is show to illustrate the signal-to-noise ratio of the isolated action potentials. **(b)** Interspike interval (ISI) histograms are shown for both neurons of each pair. Insets show the first 10ms of the ISI distribution (same vertical scale as full histograms). Note that there are no ISIs of 1ms and few ISIs of 2ms, consistent with the fact that isolation was excellent for these example neurons. **(c)** Scatter plot of z-scored responses for each pair of neurons, illustrating the significant noise correlation shown for these examples.

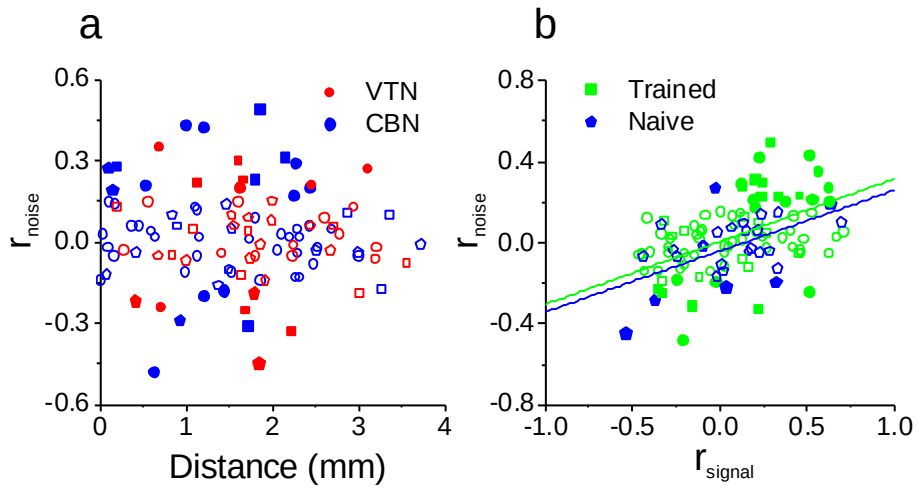

Suppl. Fig. 5. Properties of noise correlations (r_{noise}). (a) We found no significant dependence of r_{noise} (computed from the middle 400 ms of response) on the distance between simultaneously recorded neurons in either VTN or CBN (Spearman rank correlations, $p > 0.5$). **(b)** Unlike MSTd neurons, the relationship between r_{noise} and r_{signal} for VTN/CBN cells does not depend on whether the animals were trained to perform the heading discrimination task (blue: data from naïve animals, n=28; green: data from trained animals, n=82). Lines indicate linear regression fits (ANCOVA, interaction effect, p=0.9, main effect, p=0.11). For both (a) and (b), filled symbols illustrate r_{noise} values significantly different from 0 ($p<0.05$); open symbols illustrate r_{noise} values not significant different from 0 ($p>0.05$).

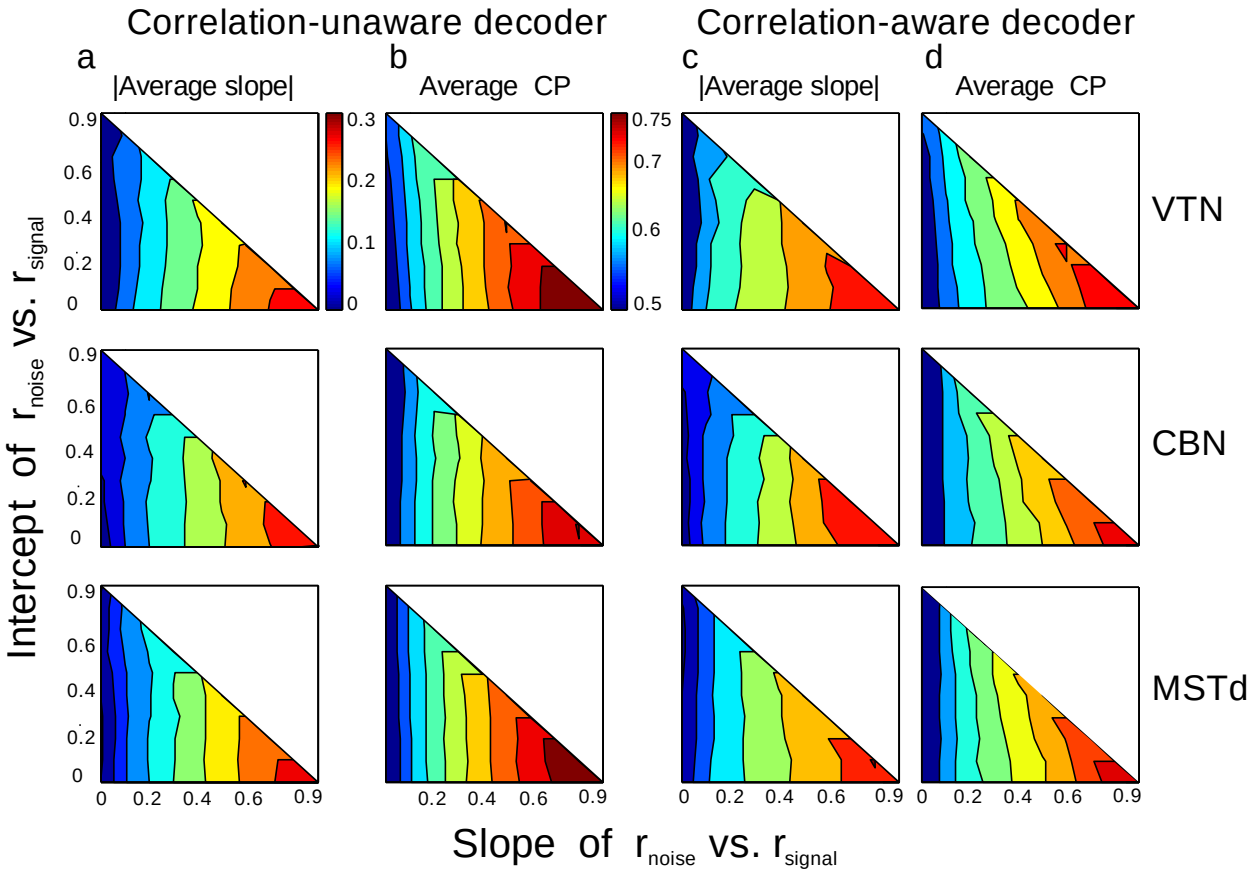

Suppl. Fig. 6. Impact of noise correlation structure on choice probability (CP) and its relationship with neuronal threshold. Color maps in columns (a) and (c) show the average slope of the relationship between choice probability (CP) and neuronal threshold (as in Fig. 8c) for a simulated population of 200 neurons. Color maps in columns (b) and (d) show the average CP of the simulated neurons. In each color map, data are plotted as a function of the slope and intercept of the relationship between r_{noise} and r_{signal}. The white region corresponds to a parameter range in which r_{noise} values exceed the allowable range of [-1 1]. Data are shown for simulated populations based on data from VTN (top row), CBN (middle row) and MSTd (bottom row). The left two columns (a, b) show results when the decoder is unaware of the interneuronal correlations; the right two columns (c, d) show results for a correlation-aware decoder. For both decoders, the average CP and slope of the threshold-CP relationship depend mainly on the slope of the relationship between r_{noise} and r_{signal}, with substantially less contribution from the intercept. Note, however, that the intercept has slightly more influence on average CP for the correlation-aware decoder (d).

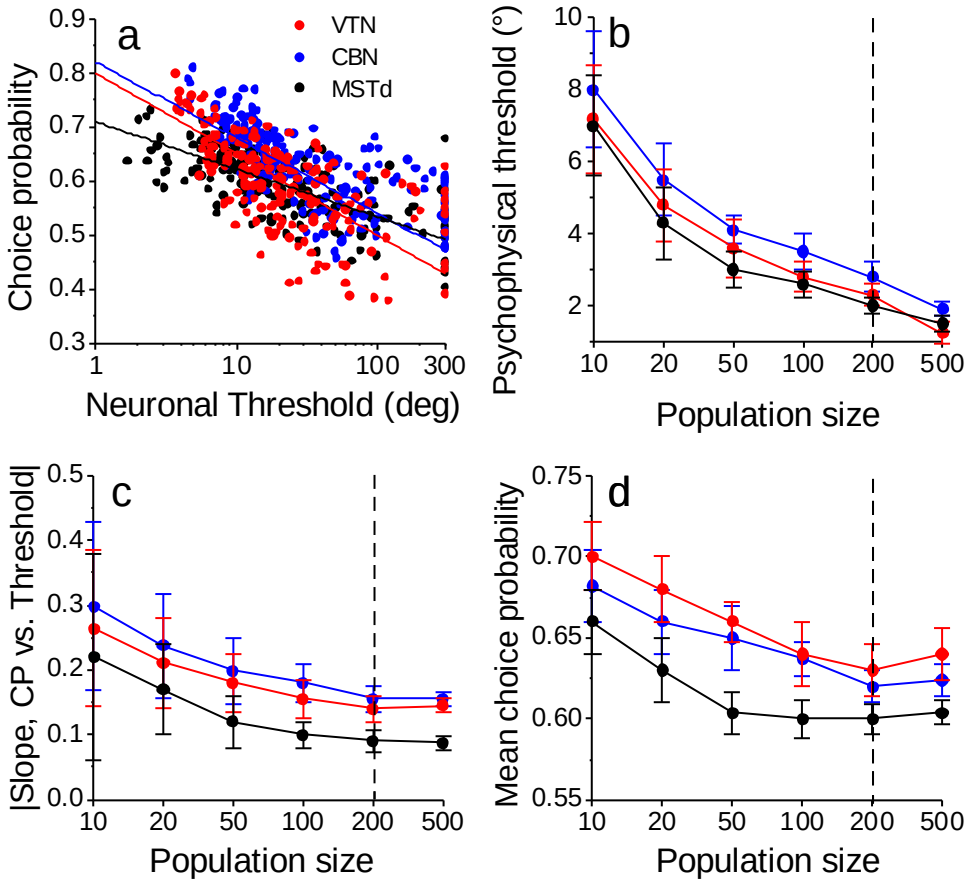

Suppl. Fig. 7. Simulation results based on an SVM decoder that is aware of the specific interneuronal correlation structure among the neurons in each simulated population. Format is identical to that of Fig. 8 in the main text. Results are also similar to Fig. 8, with the most notable exception being the dependence of predicted psychophysical threshold on population size (panel b). Note that predicted thresholds continue to decline with population size and that lower thresholds are predicted for large populations, as compared to the correlation-unaware decoder of Fig. 8.

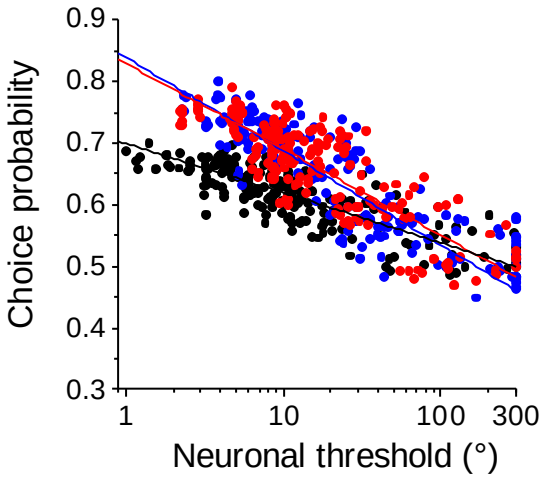

Suppl. Fig. 8. Maximum-likelihood decoder simulations. Simulation of the relationship between choice probability and neuronal threshold for different areas, based on a standard maximum likelihood decoder that assumes independent Poisson spiking statistics (see Methods). Results are qualitatively similar to those using the SVM-based decoder (Fig. 8a).

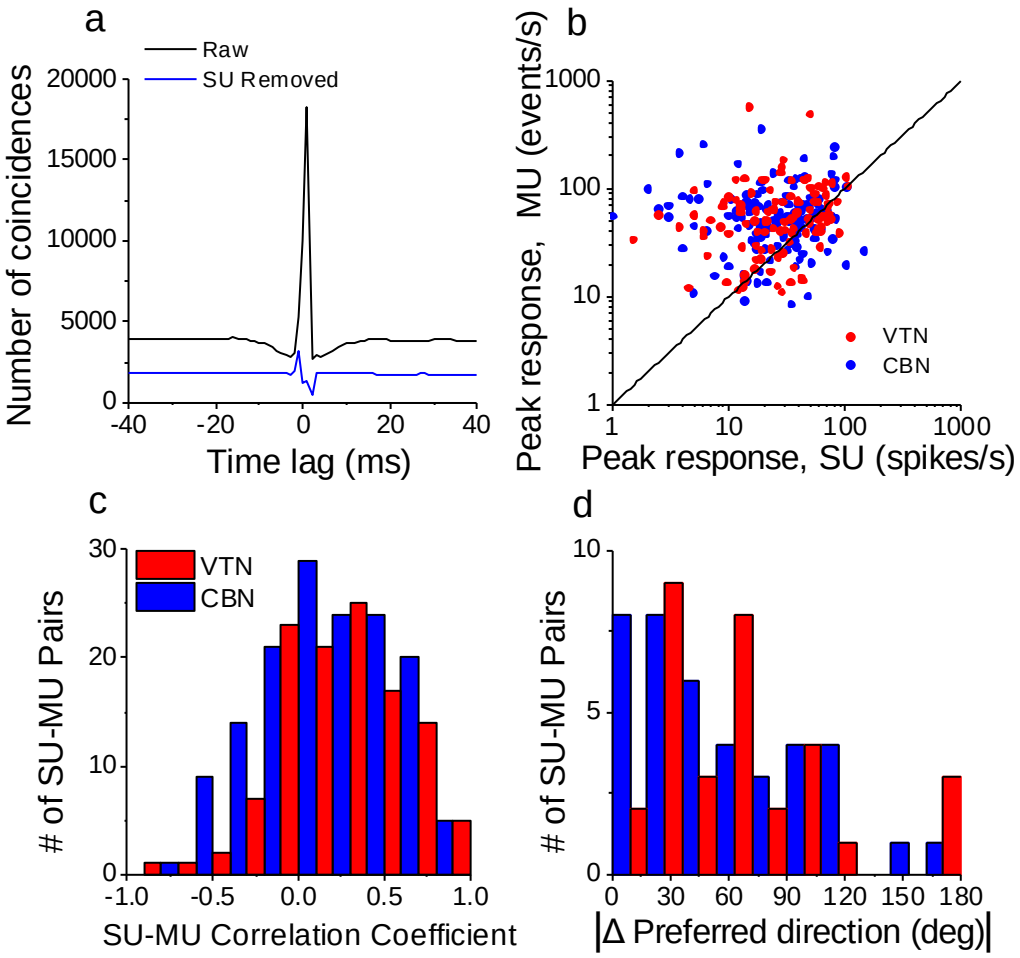

Suppl. Fig. 9. Analysis of clustering of heading tuning in VTN/CBN. For each recording site where a single unit (SU) was isolated, multi-unit (MU) activity was also extracted by thresholding the raw neural signals. **(a)** Averaged cross-correlation function for all pairs of SU and MU recordings in VTN/CBN. The black curve shows the raw average cross-correlation, and the sharp peak reflects that fact that each SU spike is included in the MU signal. The blue curve shows the average cross-correlation function after SU spikes were removed from the MU signal. The elimination of the central peak demonstrates that this operation renders the SU and MU responses essentially independent. **(b)** Comparison of SU and MU peak responses, measured during the heading tuning protocol. Each data point shows the peak MU response against the peak SU response for each neuron, after spontaneous activity is subtracted from each measure. **(c)** Distributions of correlation coefficients between SU and MU tuning profiles. The tendency toward positive values indicates that SU and MU tuning curves tend to be similar, although this clustering of tuning is weak. **(d)** Distribution of the difference in preferred directions between corresponding SU and MU responses. Data are shown here only for cases in which both SU and MU responses showed significant tuning (ANOVA, $p<0.05$). Both distributions are significantly different from uniform (permutation test, $p<0.01$), with a clear tendency toward similar tuning preferences in SU and MU responses. This clustering is modest, however, given the large spread of the differences in direction preference. CBN: blue, VTN: red.